



A Numerical Assessment of the Air Flow Behaviour in a Conventional Compact Dry Kiln

P.S.B. Zdanski[†], D.G. Possamai, and M. Vaz Jr.

Department of Mechanical Engineering, State University of Santa Catarina Campus Universitario Prof. Avelino Marcante, Joinville, 89219-710

[†] Corresponding Author Email: paulo.zdanski@udesc.br

(Received May,05,2014; accepted January,08,2015)

ABSTRACT

Convective drying is the most common drying strategy used in timber manufacturing industries in the developing world. In convective drying, the reduction rate of the moisture content is directly affected by the flow topology in the inlet and exit plenums and the air flow velocity in the channels formed by timber layers. Turbulence, boundary layer separation, vortex formation and recirculation regions are flow features that are intrinsically associated with the kiln geometry, which in turn dictate the flow velocity across the timber stack and, ultimately, the drying rate. Within this framework, this work presents a numerical study of the effects of the plenum width and inlet flow velocity in a compact dry kiln aiming to establish design recommendations to ensure the highest possible level of flow uniformity across the lumber stack. The numerical solution of the mathematical model is obtained through the finite-volume based Ansys CFX[®] flow solver. Validation of the numerical approximation is performed by comparing numerical and experimental flow velocities for a scale model of a kiln available in the literature.

Keywords: Timber drying; Compact dry kilns; Finite volumes

NOMENCLATURE

A_c	channel cross-sectional area	u_i, u_j	velocity components
i, j	indicial notation	\bar{u}_c	mean velocity in an individual channel
D_h	hydraulic diameter	u_e	entrance velocity
$I_{\Delta p}$	pressure distribution index	x_i, x_j	coordinate directions
I_u	velocity distribution index	α	kinetic energy correction factor
p	pressure	ε^{RMS}	Root Mean Square error
\bar{p}_c	mean pressure in an individual channel	μ	molecular viscosity
Q_c	channel volumetric flow rate	μ_T	turbulent eddy viscosity
Q^k	total flow rate in the kiln	λ	friction factor
R_c	hydraulic impedance	ρ	specific mass
t	time	$\Delta \bar{p}^k$	total pressure drop in the kiln

1. INTRODUCTION

A uniform air flow distribution throughout a convective dry kiln is one of the most important requirements to achieve high quality drying processes, as highlighted by [Nijdam and Keey \(2000\)](#), [Ledig et al. \(2001\)](#) and [Nijdam and Keey \(2002\)](#). Therefore, the understanding of the air flow behaviour in a dry kiln (and the related physics of the problem) is crucial for the process control and ensuing product quality.

The number of works reporting studies on the ef-

fects of air flow in drying processes (not necessarily in convective dry kilns) has increased in recent years. An experimental assessment of the effects of distinct entrance sections on the velocity distribution in a kiln scale model was discussed by [Nijdam and Keey \(2002\)](#). More details about this important work will be given in next sections (validation of the numerical approximation). A numerical solution of the flow distribution in a convective dry kiln was presented by [Langrish \(2002\)](#), who approached the influence of the effective (bulk) viscosity upon the flow pattern using the commer-

cial code CFDS-CFX4.2[®]. Margaris and Ghiaus (2006) simulated extensively the air flow inside an industrial tray dryer. According to the authors, the predicted parameters for different configuration contributed to the optimization of the drying space and led to a substantial improvement of the quality of the dried product. Kaya *et al.* (2008) addressed the air flow problem inside a simplified kiln geometry (a single rectangular moist object in a rectangular channel) using the Fluent[®] commercial CFD flow solver. Various dryer configurations were studied by the authors, being the most effective the one that the flow impacts directly against the moist object. More recently, a 3D computational modelling of laminar external flow over a single moist object placed in a rectangular channel subjected to convective drying was studied by Mohan and Talukdar (2010). The authors indicated that by increasing the air velocity by three times, the drying rate can be increased approximately by 43 %. Younsi *et al.* (2010) utilised a 3D model to compute the turbulent flow inside convective kilns, comparing the numerical results with experimental data. The authors solved the air flow problem for a single kiln geometry using the commercial software ANSYS-CFX[®]. Ghiaus *et al.* (2010) adopted also the Fluent[®] commercial CFD code to predict the air flow field inside an empty and pallet loaded industrial dryer. Improvement of airflow distribution was achieved by different arrangements of the pallet stacks as well as by using screen walls. Lamnatou *et al.* (2010) investigated numerically the effect of the relative positioning of a pair of porous blunt plates inside a rectangular channel subjected to convective drying on heat/mass transfer phenomena. The results show that the side-by-side arrangement provided the best overall drying behaviour, owing to the enhancement of heat/mass transfer caused by the blockage effect. The effect of the velocity distribution across the timber stack on the drying rates for different dry kiln configurations was discussed by Vaz Jr. *et al.* (2013) based on a global-local conjugated heat and mass transfer model. The authors follow Nijdam and Keey (2000) and Ledig *et al.* (2001) who approach the air flow problem using the one-dimensional head loss equation to compute channel velocities across the timber stack.

The paramount importance of the flow pattern and velocity magnitudes in convective dry kilns contrasts with the relatively few studies (when compared to other fluid flow problems) devoted assess the effects of the kiln geometric configurations in the air flow distributions. It is well known that flow maldistribution across timber stacks in kilns cause unacceptable variations in drying rates (Nijdam and Keey 2000) and consequent undesirable defects, such as rupture of the wood tissue, warp, uneven

final moisture content and discoloration (Simpson 2001). Notwithstanding, it is expected that the geometric configuration of a compact dry kiln, as well as lumber stacking, affect both the head loss and flow behaviour. Following this route, the present work aims at studying numerically the effects of the plenum width and inlet flow velocity associated with a conventional dry kiln aiming to establish design recommendations to ensure the highest possible level of flow uniformity across the lumber stack. A two-dimensional approximation of the dry kiln was used in the simulations. The main results indicate that the plenum size (geometric aspect) affects drastically the flow uniformity inside the kiln.

2. THEORETICAL FORMULATION

Governing equations: The mathematical model adopted is the classical Reynolds Average Navier-Stokes equations (RANS) subjected to the Boussinesq turbulent eddy viscosity hypothesis. Within this framework, the time averaged conservation principles of mass and linear momentum in indicial notation are given by

$$\frac{\partial u_i}{\partial x_i} = 0, \quad (1)$$

$$\frac{\partial(\rho u_i)}{\partial t} + \frac{\partial(\rho u_j u_i)}{\partial x_j} = \frac{\partial p}{\partial x_i} + \frac{\partial}{\partial x_j} \left[(\mu + \mu_T) \left(\frac{\partial u_i}{\partial x_j} + \frac{\partial u_j}{\partial x_i} \right) \right], \quad (2)$$

The parameters u_i and p in the preceding equations represent average quantities, i.e, velocity components and pressure. Furthermore, for computing the turbulent eddy viscosity, μ_T , the classical two-equation $k - \epsilon$ turbulence model (Launder and Spalding 1974) is employed. The boundary conditions used in the simulations are as follows: the turbulent kinetic energy and its dissipation rate at the entrance section are $k_e = 0.04 (1/2 u_e^2) J/kg$ and $\epsilon_e = 392 J/kg s$ (Zdanski *et al.* 2005), respectively, the pressure at the exit section is 101.3 kPa, being assumed a prescribed entrance velocity, u_e , at the inlet plenum and null velocities at the solid walls.

It is noteworthy that this mathematical approach has been largely used in industrial applications. Robustness and good approximation to the physical phenomena have encouraged its use in problems ranging from slotted blade in compressors (Ramzi and AbdErrahmane 2013) to dryers (see, for instance, the aforementioned works of Langrish (2002), Margaris and Ghiaus (2006), Kaya *et al.* (2008), Younsi *et al.* (2010) and Ghiaus *et al.* (2010)). The authors have also successfully implemented this model in an in-house computational

code to solve forced convection in solar panels enclosures (Zdanski *et al.* 2005).

Numerical discretization method: The set of governing equations is solved numerically through the commercial ANSYS CFX[®] code. The CFX[®] software employs the so-called Element based Finite Volume Method to discretize the governing equations for both structured and unstructured meshes. The pressure-velocity coupling strategy used by the code is based on collocated meshes. The numerical strategy employed in the code was initially proposed by Rhie and Chow (1983), who defined higher order interpolation functions at the finite volume surfaces in order to avoid the odd-even decoupling problem. The overall solution procedure is very similar to the classical SIMPLE algorithm (Patankar 1980), so that the convection and diffusion terms are discretized according to the well-known hybrid scheme, i.e., the diffusion terms are evaluated with central discretization while the convection terms interchange between upwind and central-differencing discretization according to the value of the grid cell Peclet number (Patankar 1980). The resulting set of algebraic equations is solved by an iterative procedure known as partial LU decomposition technique.

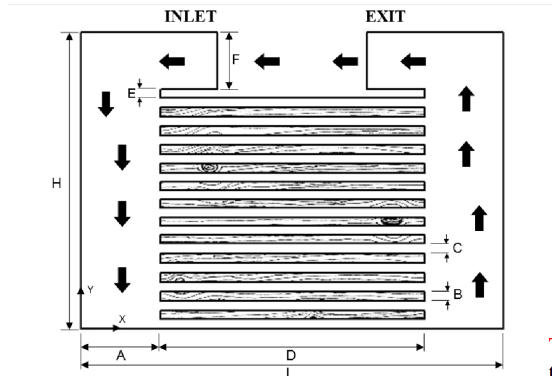


Fig. 1. Geometry of the compact dry kiln (represented out-of-scale).

3. VALIDATION OF THE NUMERICAL APPROXIMATION

The flow structure of a dry kiln is complex owing to the presence of boundary layer separation and vortices, thereby requiring a robust approach to pressure velocity coupling and turbulence modelling. Therefore, validation is essential to ensure credibility of the numerical predictions. For the sake of objectivity, this text only presents comparisons between numerical simulations and experimental results provided by Nijdam and Keey (2002) for a kiln scale model. The experimental apparatus consists of a water-test facility in a closed-circuit arrangement. The water is pumped at a con-

trolled flow rate from the reservoir tank up to the flow header tank and hydraulic kiln. The hydraulic kiln is made of Perspex to enable visualisation of the flow field. Cavitation-induced bubbles and the hydrogen-bubble method were used for visualisation purposes. Velocities were measured inside the hydraulic kiln and presented for the odd channels as relative velocities, \bar{u}_c/u_e , where \bar{u}_c is the mean velocity in a single channel and u_e is the inlet velocity. Figure 1 shows the general outline of a kiln and Table 1 presents the corresponding geometrical data used in Nijdam and Keey (2002). The high Reynolds $k - \epsilon$ model was used in the simulations with uniform entrance velocity, $u_e = 4.2$ m/s.

Table 1. Kiln geometrical data: Nijdam and Keey (2002) reduced scale model.

Description	Symbol	Value
Plenum height	H	0.26 m
Plenum width	A	0.090025 m
Entrance channel height	F	0.065 m
Inlet neck	E	0.1 m
Stack width	D	0.3 m
Kiln width	L	0.48005 m
Lumber thickness	B	0.01 m
Channel height	C	0.05 m

The mesh effect upon the numerical solution is also evaluated by defining (a) three uniform meshes with progressive refinement and (b) three non-uniform meshes with a maximum 10 % stretch ratio in the x direction (with grid concentration close to critical regions) and uniform in the y direction. Table 2 indicates the mesh sizes whereas Figure 2 illustrates a typical topology for the stretched meshes close to the entrance channel and inlet plenum. It is noteworthy that the meshes were defined ensuring that the dimensionless distance of the closest nodes to the solid surfaces, y^+ , satisfies the conditions required by the turbulence model used in the simulations.

Table 2. Assessment of mesh dependency.

	Mesh	Size	$\epsilon_{\bar{u}_c/u_e}^{RMS} \times 10^2$
Uniform	#1	621,044	8.66691
	#2	777,524	8.34767
	#3	1,261,724	8.02831
Non-uniform	#4	121,584	7.78484
	#5	143,656	7.46861
	#6	214,376	7.40015

The simulations show a good agreement between

the numerical and experimental relative velocities across the stack height for all meshes, as indicated in Fig.3 (one cannot visually distinguish the values obtained for different meshes). The Root Mean Square error, $\epsilon_{\bar{u}_c/u_e}^{RMS}$, between the numerical and experimental relative channel velocities for the respective meshes are also presented in Table 2. The results indicate two main conclusions: (i) The RMS errors between numerical and experimental channel velocities were very small for all meshes, with a somewhat better performance of the non-uniform meshes; (ii) the RMS error slightly decreases when meshes are refined for the range of uniform and non-uniform mesh sizes simulated. Such results indicate no inconsistencies of the numerical approximation or pathological mesh dependency for the present application.

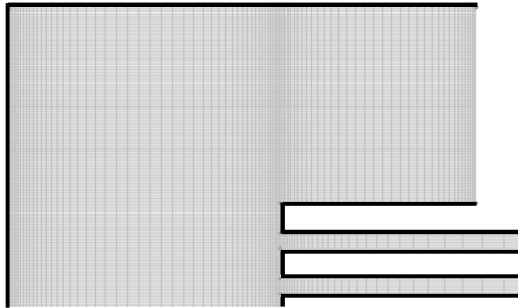


Fig. 2. Illustration of a typical non-uniform mesh for the entrance channel and inlet plenum.

The simulations indicate also good qualitative agreement with Nijdam and Keey (2002) experimental measurements. The streamlines in the inlet plenum for the test case is presented in Fig.3, which reproduce almost exactly the experimental flow topology pictured by Nijdam and Keey (2002). In this example, the flow features are quite distinctive: in addition to the vortices located in the top and bottom corners of the inlet plenum, a third vortex is formed near the entrance of the top three channels with its centre aligned to channel 12. This vortex is formed by flow separation in the convex corner of the entrance channel causing velocities in the flow channels 10 – 13 to decrease, as observed in Fig.3 for the relative velocity, \bar{u}_c/u_e .

4. FULL SCALE SIMULATIONS: ASSESSMENT AND DISCUSSIONS

The physics involved in convective drying of timber is very complex owing to different phenomena involved. Simulation of timber dehumidification depends upon a fully coupled solution of the momentum, energy and mass conservation equations. Furthermore, mechanical deformation such as warping requires solution of a coupled mechanical problem.

In general, temperature and moisture content, allied to heat and mass convection coefficients are the most important variables to be controlled in a convective dry kiln. On the other hand, all such variables are directly dependent upon the flow velocity near the timber surfaces (Nijdam and Keey 2000). For instance, high velocities cause the heat transfer and mass transfer convection coefficients to increase, thereby affecting heat and mass diffusion in the wood and increasing the drying rate. The kiln operator must, therefore, (1) set the flow circulation rate and (2) arrange properly the timber load to ensure a uniform flow distribution across the stack height. In order to maximise the timber load, the operator may be tempted to leave little room for air circulation (small plenum size) or else to increase air flow to speed up drying (inlet velocity). Such practices may cause air flow maldistribution, leading to different drying rates across the timber stack. Notwithstanding, one should balance increasing productivity and product quality by observing certain limits. Therefore, a great effort has been devoted to investigate velocity distribution in dry kilns and its importance has been translated by the fact that many works (Nijdam and Keey 2000; Ledig *et al.* 2001; Langrish 2002; Margaris and Ghiaus 2006) have been focused solely on studying the flow behaviour in dryers.

There are several factors which affect the flow behaviour in compact dry kiln, such as inlet velocity, plenum width, stack height and width, lumber thickness and channel height amongst others. However, the experimental works reported by Ledig *et al.* (2001) and Nijdam and Keey (2000) indicate that inlet velocities and plenum size impose the largest effects upon the flow topology in a typical industrial dry kiln. Therefore, for the sake of objectivity, this work is focused solely on assessing the effect of these parameters on the velocity distribution in a conventional dry kiln.

As mentioned in previous sections, drying rate is mostly affected by the magnitude of air velocity close to the moist surface. Therefore, in order to ensure a homogeneous drying, the kiln design and flow settings must favour flow uniformity. The basic geometrical model is shown in Fig.1 and the full scale kiln dimensions are indicated in Table 3. The compact design is motivated by applications of small and medium size lumber manufacturers common in the developing world.

The numerical approach used in the example follows the general concept described in the validation section. Three plenum sizes are investigated, $A = 100, 150$ and 300 mm, for inlet velocities $3 \leq u_e \leq 9$ m/s. Owing to the mesh-dependency study presented in section 3., non-uniform structured meshes

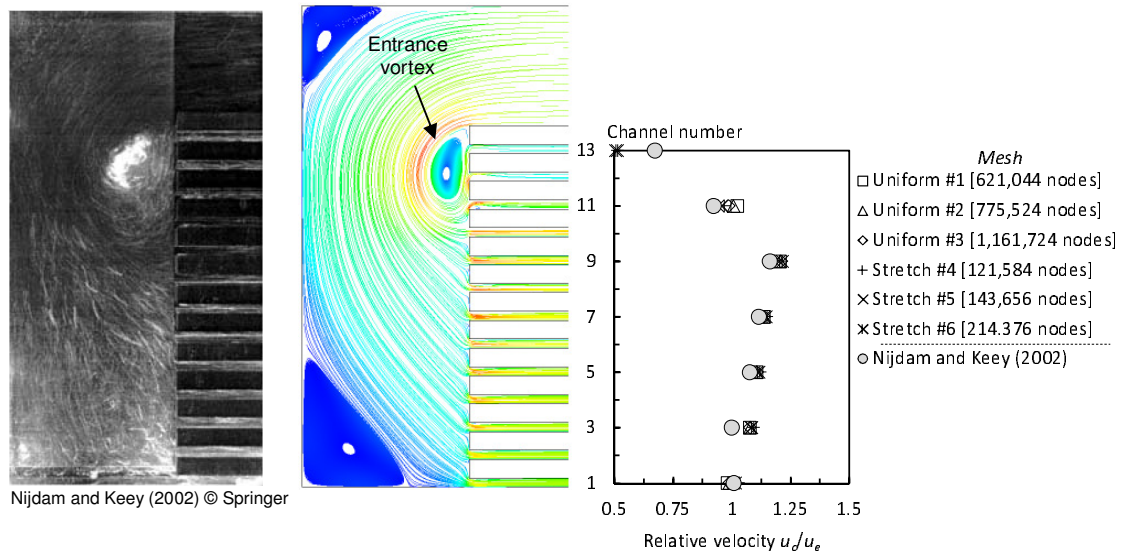


Fig. 3. Flow topology in the inlet plenum and relative channel velocity \bar{u}_c/u_e across the stack height.

with 358,876, 392,196 and 462,364 nodes were respectively used to simulate dry kilns with the aforementioned plenum sizes.

Table 3. Compact dry kiln geometrical data.

Description	Symbol	Value
Plenum height	H	0.5875 m
Plenum width	A	100/150/300 mm
Entrance channel height	F	0.1 m
Inlet neck	E	0.0125 m
Stack width	D	1.6 m
Kiln width	L	1.9 m
Lumber thickness	B	0.025 m
Channel height	C	0.0125 m

4.1 The effects of the plenum size and entrance velocity

Drying is accomplished by air flow in channels bounded by upper and lower timber layers and spaced by stickers of a given height, C . In order to ensure velocity uniformity across the timber stack, pressure equalisation at entrance and exit of the flow channels is required, which constitutes the main purpose of the inlet and exit plenums. Figure 4(a) shows a typical flow topology for a plenum size $A = 150$ mm and entrance velocity $u_e = 5$ m/s. The streamlines indicate recirculation in all corners of the inlet and exit plenums, and a typical vortex near the top channels at the inlet plenum (referred here as *entrance vortex*). A jet-type flow, characteristic of sudden expansions, appears at each channel exit, leading to formation of a confined recirculation flow. The pressure distribution (shown in the figure as pressure difference, $\Delta p = p - \bar{p}_{exit}$) is pre-

sented in Fig.4(b). It can be clearly observed that the low pressure region in the inlet plenum is associated with the vortex formed in the same location.

The influence of the plenum width is illustrated in Fig.5, which presents streamlines for plenum sizes $A = 100, 150$ and 300 mm and entrance velocity $u_e = 5$ m/s. It can be identified a typical flow pattern for the basic geometrical design of the compact dry kiln regardless the plenum width. Notwithstanding, Fig.5 shows that the entrance vortex is closer to the timber stack for narrower plenums, increasing its effects upon the channel velocities. Therefore, larger plenums make possible the reverse flow to feed the top channels, leading to more uniform velocity distributions across the stack height.

The mean pressure difference, $\Delta \bar{p}_c = \bar{p}_c^i - \bar{p}_c^e$, and velocity, \bar{u}_c , in each flow channel are presented in Fig.6(a) and 6(b), respectively, for plenum sizes $A = 100, 150$ and 300 mm and entrance velocity $u_e = 5$ m/s. The smaller pressure associated to the entrance vortex (see Fig.4) constitutes an actual obstruction to flow which is translated into relevant changes in pressure drop and velocity for the channels facing the recirculation. It can be observed that the level of pressure drop and velocity inhomogeneity across the timber stack increases for narrower plenums.

The influence of the entrance velocity is investigated for $3 \leq u_e \leq 9$ m/s. The flow topology for this range of velocities is very similar to those illustrated in Fig.5, i.e., confined recirculation zones in all corners of the inlet and exit plenums and a vortex located close to the top flow channels. The results indicate a typical physical behaviour of flow problems, i.e., larger entrance velocities, u_e , mag-

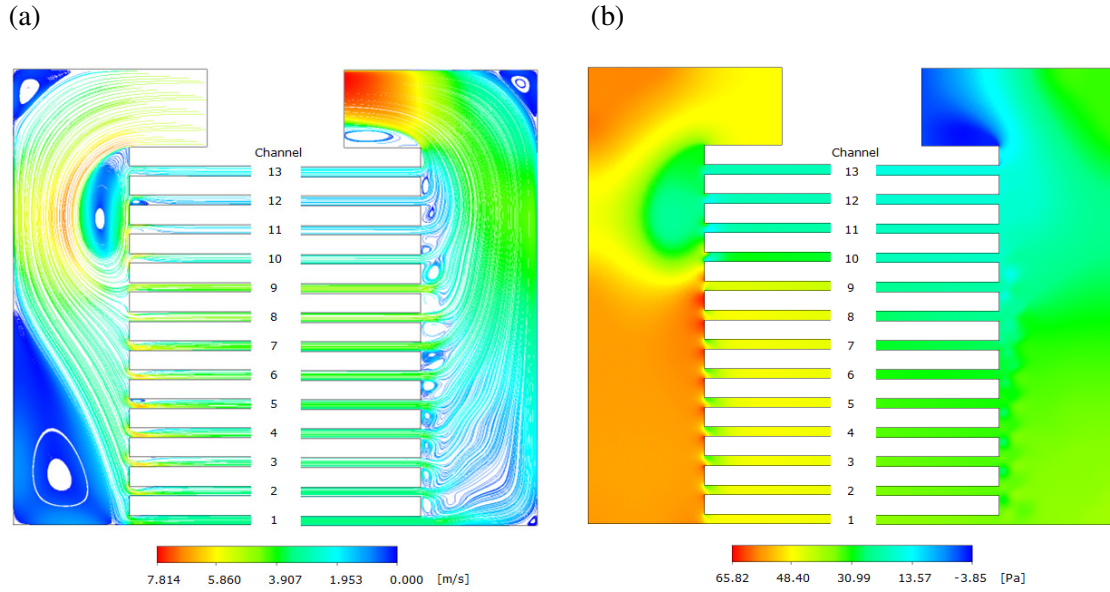


Fig. 4. (a) Streamlines featuring velocity magnitude, $|\mathbf{v}|$, and (b) Relative pressure, $\Delta p = p - \bar{p}_{exit}$, for a plenum width $A = 150$ mm.

nify the effects of the entrance vortex (low pressure zone), causing the absolute difference of pressure drop and velocities across the stack height to increase, as illustrate Fig.s7(a) and 7(b) for a plenum width $A = 150$ mm. However, great care should be exercised when assessing the effects of the entrance velocity since higher absolute differences for larger entrance velocities, u_e , do not necessarily indicate higher inhomogeneity. It is also interesting to note that the entrance vortex is encapsulated by a region of a somewhat sharp pressure transition (clearly observed in Fig.4(b)) which causes the higher pressures close to channel 9 shown in Fig.s 6(a) and 7(a). Therefore, such pressure distribution causes velocity in the top channels to vary from small (caused by the low pressure vortex) to high (caused by the high pressure envelope) values.

Quantification of the plenum width and entrance velocity influences is performed by the pressure variation and velocity variation indices, which represent, respectively, the ratio between the maximum amplitude of the pressure drop and channel velocity and corresponding mean values,

$$I_{\Delta p} = \frac{\Delta \bar{p}_c^{max} - \Delta \bar{p}_c^{min}}{\Delta \bar{p}_c^{mean}} \text{ and } I_u = \frac{\bar{u}_c^{max} - \bar{u}_c^{min}}{\bar{u}_c^{mean}}, \quad (3)$$

where the superscripts *max* and *min* indicate maximum and minimum channel pressure drop/velocity, and $\Delta \bar{p}_c^{mean}$ and \bar{u}_c^{mean} are the mean pressure drop and mean velocity across the stack height. Table 4 presents the indices for plenum widths $A = 100$, 150 and 300 mm and entrance velocities $3 \leq u_e \leq 9$ m/s. The results highlight two important aspects:

(a) Narrow plenums indeed lead to higher flow non-uniformity.

(b) Higher entrance velocities for the same plenum size do not significantly affect flow homogeneity.

Table 4 shows that, for the same plenum width, both pressure variation and velocity variation indices do not present significant changes. For instance, for a plenum size $A = 150$ mm, the indices are approximately $I_{\Delta p} \approx 1.53$ and $I_u \approx 0.90$ for all entrance velocities. Once the flow non-uniformity is acceptable to a given global flow rate, this prediction gives greater assurance to the dry kiln operator that adjustments in the flow rate to match different drying schedules will not cause significant velocity differences (with respect to the mean velocity) which would compromise the product quality. On the other hand, the plenum width is of paramount importance to evaluate flow uniformity. Table 4 indicates that both pressure and velocity variation indices, $I_{\Delta p}$ and I_u , present relevant changes with plenum width. The simulations show that, for plenum sizes $A = 300$, 150 and 100 mm, the average indices increase as $I_{\Delta p} \approx 1.35$, 1.53 and 2.15, and $I_u \approx 0.67$, 0.90 and 1.24, i.e., the velocity non-uniformity increases around 85 % when the plenum size is reduced from 300 to 100 mm.

4.2 Global assessment of the compact dry kiln

The complex flow pattern obtained by the simulations recommends further consistency verification in order to identify possible discrepancies or even model incompatibility within the range of entrance velocities, u_e , and plenum sizes, A . The global assessment of the numerical solutions is performed

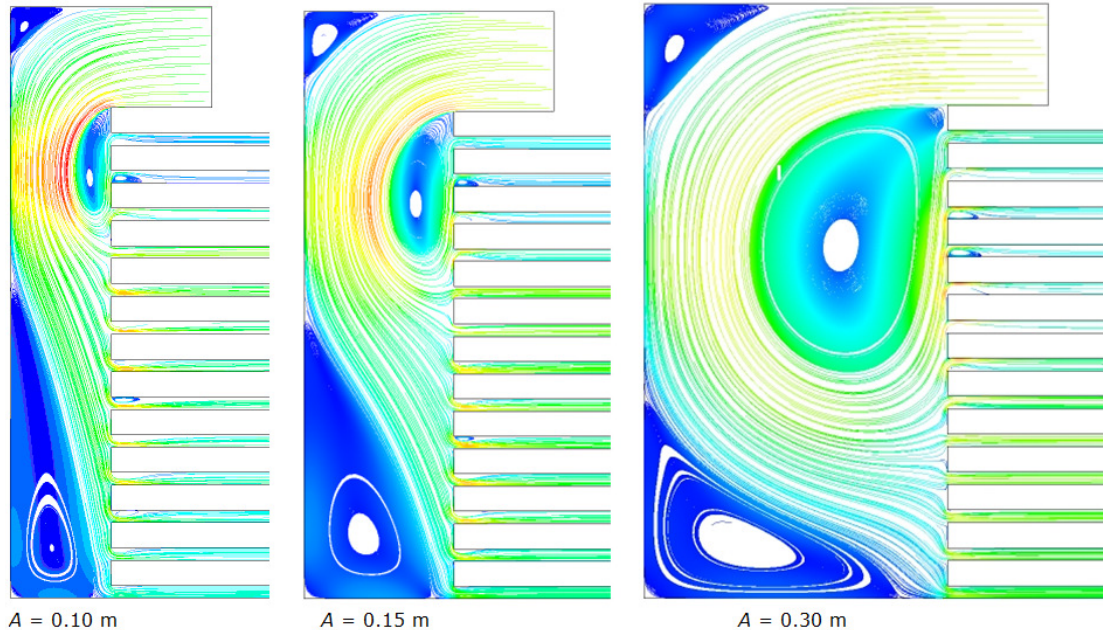


Fig. 5. Flow topology: streamlines at the inlet plenum for $A = 100, 150$ and 300 mm.

Table 4. Compact dry kiln geometrical data.

Index	u_e [m/s]	A [mm]		
		100	150	300
$I_{\Delta p}$	3	2.060	1.486	1.297
	5	2.180	1.534	1.391
	7	2.198	1.567	1.305
	9	2.145	1.518	1.389
I_u	3	1.194	0.8565	0.6441
	5	1.239	0.8988	0.6710
	7	1.265	0.9148	0.6847
	9	1.273	0.9192	0.6874

by the head loss equation (Post 2011) written for the pressure drop in each flow channel, $\Delta \bar{p}_c$,

$$\begin{aligned} \Delta \bar{p}_c &= \bar{p}_i - \bar{p}_e \\ &= \left[\frac{\rho \alpha_i}{2A_c} - \frac{\rho \alpha_e}{2A_c} + \lambda \frac{\rho}{2A_c} \frac{D}{D_h} \right] Q_c^2, \quad (4) \\ &= R_c Q_c^2 \end{aligned}$$

where subscripts i and e indicate entrance and exit sections of each individual channel, α is the kinetic energy correction factor, ρ is the specific mass, A_c is the cross-sectional area, $Q_c = \bar{u}_c A_c$ is the channel volumetric flow rate, λ is the friction factor, D is the channel length, D_h is the hydraulic diameter, and R_c is the hydraulic impedance.

A correlation between pressure drop, $\Delta \bar{p}_c$, and flow rate, Q_c , for each channel is performed for all

plenum sizes and entrance velocities. In spite of the differences which A and u_e impose upon the local velocity and pressure distributions, the simulations show a small dispersion around the curve $\Delta \bar{p}_c = R_c Q_c^2$ presented in Fig.8. A curve-fitting procedure indicates that the hydraulic impedance is $R_c = 9.0567 \times 10^3 \text{ Pa}/(\text{m}^3/\text{s})^2$ with a coefficient of determination $R^2 = 0.986$. The results indicate a small variability within an acceptable range of the flow parameters of Equation 4, which reflects the consistency of the proposed numerical approximation.

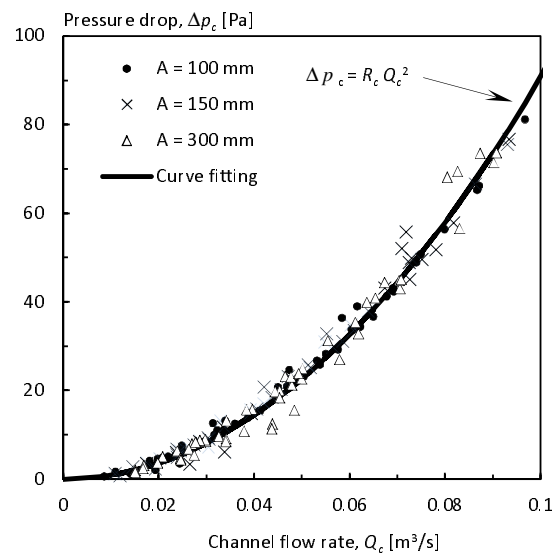


Fig. 8. Channel pressure drop, $\Delta \bar{p}_c$, vs. flow rate Q_c , for all plenums and inlet velocities.

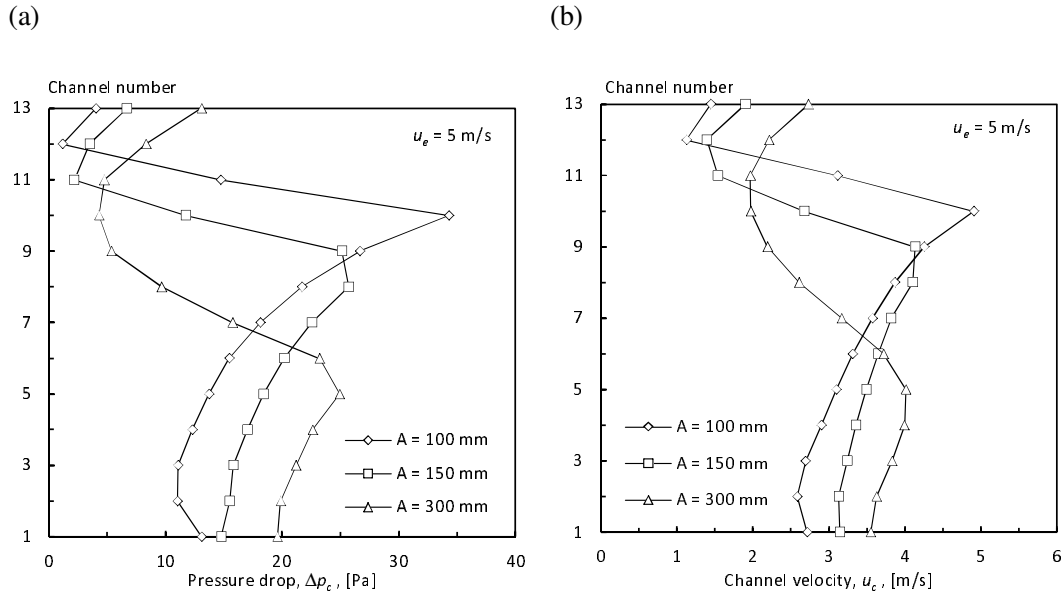


Fig. 6. Channel (a) pressure drop, $\Delta \bar{p}_c$, and (b) velocity, \bar{u}_c , for plenum widths $A = 100, 150$ and 300 mm and inlet velocity $u_e = 5$ m/s.

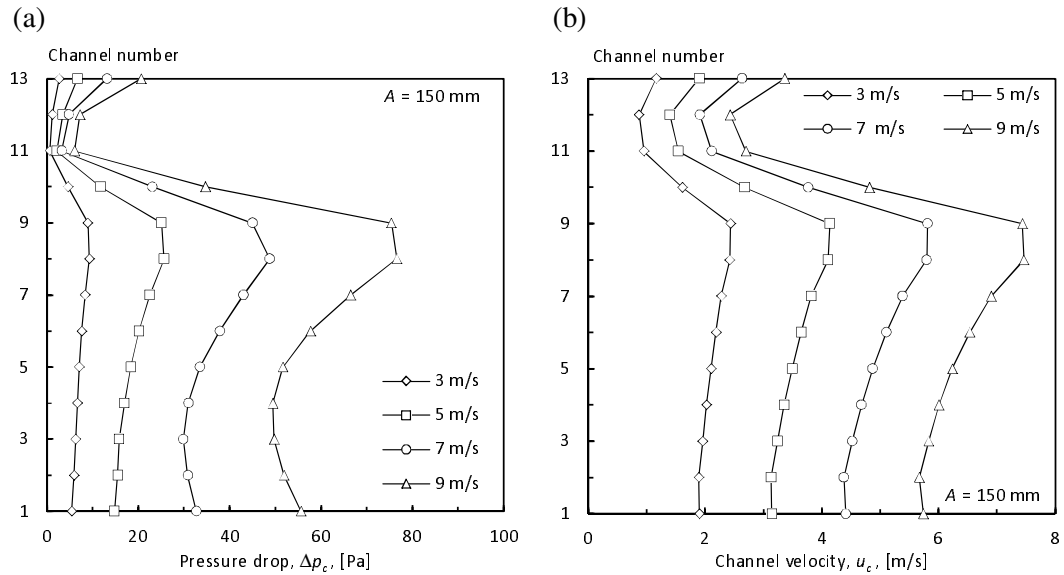


Fig. 7. Channel (a) pressure drop, $\Delta \bar{p}_c$, and (b) velocity, \bar{u}_c , for plenum widths $A = 150$ mm and inlet velocity $u_e = 3, 7$ and 9 m/s.

It is important to note that the pressure drop – flow rate correlation discussed in the previous paragraphs is valid only for flow in the channels bounded by the upper and lower timber layers. The overall dry kiln head loss must account for energy dissipation in flow separation and vortices, change of flow direction in the inlet / exit plenums, and contraction / expansion at the entrance / exit of the flow channels across the timber stack. Therefore, the effects of the pressure drop in the inlet and exit plenums contribute to the overall air flow behaviour of the compact dry kiln and suggest an individual assessment, as presented in Fig.9 for plenum sizes $A = 100, 150$ and 300 mm.

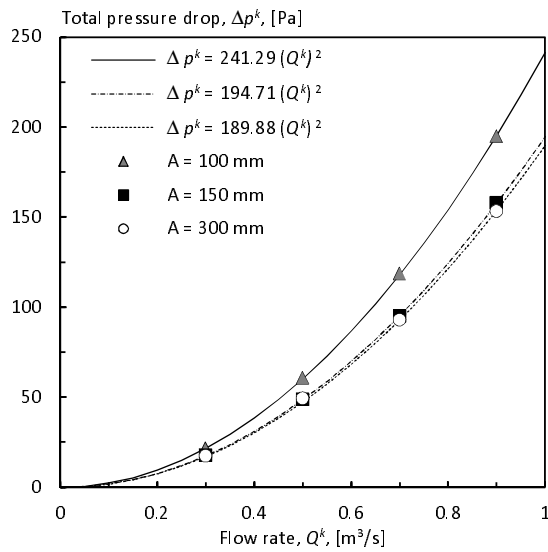


Fig. 9. System behaviour: total pressure drop, $\Delta \bar{p}^k$, vs. global flow rate Q^k , in the dry kiln.

The correlation between the total pressure drop in the dry kiln, $\Delta \bar{p}^k = \bar{p}_{inlet} - \bar{p}_{exit}$, and corresponding flow rate, $Q^k = A^{inlet} u_e$, for each plenum size follows the typical behaviour of the so-called system approach, $\Delta \bar{p}^k = R^k (Q^k)^2$, in which R^k is the system impedance. The individual curves and values of for the respective plenum sizes are indicated in Fig.9 (the coefficient of determination of each curve is approximately $R^2 = 0.9998$). The numerical results show two interesting aspects:

(a) The influence of the plenum size upon the global air flow behaviour becomes more relevant for smaller ratios of the plenum width, A , and flow channel height, C , i.e., $A/C < 8$ for the present compact dry kiln configuration. For instance, for the same flow rate, when A/C decreases from 24 to 12 and from 12 to 8 the global pressure drop increases 2.5 % and 23.9 %, respectively.

(b) From the global viewpoint, no significant pressure drop differences are found for inlet/exit plenums larger than 150 mm ($A/C = 12$); however,

the kiln designer must attempt to the level of flow uniformity required by the product.

5. FINAL REMARKS

Convective dry kilns have been largely used to timber drying due to the combination of low cost and technological simplicity. The drying process consists of controlled heated air flow through timber layers spaced by stickers of a given height. A certain level of velocity uniformity across the timber stack is required to ensure drying homogeneity and to prevent defects such as warping, checks, splits and discoloration amongst others. The present work has focused solely on the effects of the plenum size and global flow rate upon distribution of the flow velocity across the stack height in conventional dry kilns. The following issues were found relevant in the present analysis:

(a) the numerical model was validated against experimental results available in the literature (Nijdam and Keeey 2002) for a kiln scale model and was found appropriate to simulate this class of problems;

(b) the typical flow topology consists of large vortices located at all concave corners of the inlet and exit plenums and a vortex formed near the top channels (entrance vortex) of the timber stack in the inlet plenum;

(c) the plenum size affects significantly the entrance vortex, which in turn, induces velocity variations across the timber stack: narrow plenums cause the channel velocity non-uniformity to increase;

(d) higher global flow rates for the same plenum sizes do not necessarily increase the channel velocity non-uniformity: the dry kiln operator can adjust the global flow rate to match different drying schedules without increasing the ratio between velocity differences across the stack height and the mean channel velocity;

(e) for a given global flow rate, the global pressure drop in the compact dry kiln is significantly affected by smaller ratios between the plenum width and flow channel height, i.e., the contribution of the pressure drop in the inlet/exit plenums becomes relevant when compared to the pressure drop in the flow channels across the timber stack.

Finally, for the present compact dry kiln configuration, the simulations show that the global air flow behaviour does not change significantly for plenums larger than 150 mm, however the kiln designer must attempt to the level of flow uniformity required by the target product.

ACKNOWLEDGMENTS

The authors acknowledge the financial support provided by the Brazilian funding agency CNPq - (National Council for Scientific and Technological Development).

REFERENCES

- Ghiaus, A.G., A. Filios, D.P. Margaris, and D. Tzempelikos (2010, October). Industrial drying of wooden pallets - CFD analysis of air flow. In *Proceedings of the 17th International Drying Symposium*, Magdeburg, Germany.
- Kaya, A., O. Aydin, and I. Dincer (2008). Heat and mass transfer modeling of recirculating flows during air drying of moist objects for various dryer configurations. *Numerical Heat Transfer - Part A* 53, 18–34.
- Lamnatou, Chr., E. Papanicolaou, V. Belessiotis, and N. Kyriakis (2010). Numerical study of the interaction among a pair of blunt plates subject to convective drying – a conjugate approach. *International Journal of Thermal Science* 49, 2467–2482.
- Langrish, T.A.G. (2002). Progress in the modelling of air flow patterns in timber kilns. *Drying Technology* 20, 1789–1802.
- Lauder, B.E. and D.B. Spalding (1974). The numerical computation of turbulent flows. *Computer Methods in Applied Mechanics and Engineering* 3, 269–289.
- Ledig, S.F., J.J. Nijdam, and R.B. Keey (2001). Airflow distributions in the fillet spaces of a timber stack. *Drying Technology* 19, 1697–1710.
- Margaris, D.P. and A.G. Ghiaus (2006). Dried product quality improvement by air flow manipulation in tray dryers. *Journal of Food Engineering* 75, 542–550.
- Mohan, V.P.C. and P. Talukdar (2010). Three dimensional numerical modeling of simultaneous heat and moisture transfer in a moist object subjected to convective drying. *International Journal of Heat and Mass Transfer* 53, 4638–4650.
- Nijdam, J.J. and R.B. Keey (2000). The influence of kiln geometry on flow maldistribution across timber stacks in kilns. *Drying Technology* 18, 1865–1877.
- Nijdam, J.J. and R.B. Keey (2002). An experimental study of airflow in lumber kilns. *Wood Science and Technology* 36, 19–26.
- Patankar, S. (1980). *Numerical heat transfer and fluid flow*. Washington, USA: Hemisphere.
- Post, S. (2011). *Applied Computational Fluid Mechanics*. Sudbury, USA: Jones and Bartlett.
- Ramzi, M. and G. AbdErrahmane (2013). Passive control via slotted blading in a compressor cascade at stall condition. *Journal of Applied Fluid Mechanics* 6, 571–589.
- Rhie, C.M. and W.L. Chow (1983). Numerical study of the flow past an airfoil with trailing-edge separation. *AIAA Journal* 21, 1525–1532.
- Simpson, W. (2001). *Dry kiln operator's manual - USDA Agricultural Handbook AH-188*. Madison, USA: USDA.
- Vaz Jr., M., P.S.B. Zdanski, R.F. Cerqueira, and D.G. Possamai (2013). Conjugated heat and mass transfer in convective drying in compact wood kilns: a system approach. *Advances in Mechanical Engineering* 2013, 1–12.
- Younsi, R., D. Kocaefe, S. Poncsak, and Y. Kocaefe (2010). Computational and experimental analysis of high temperature thermal treatment of wood based on thermowood technology. *International Communications in Heat and Mass Transfer* 37, 21–28.
- Zdanski, P.S.B., M. Ortega, and N.G.C.R. Fico Jr. (2005). Heat transfer studies in the flow over shallow cavities. *Journal of Heat Transfer* 127, 699–712.